Photocatalytic degradation of levofloxacin by a novel Sm_6WO_{12}/g-C_3N_4 heterojunction: Performance, mechanism and degradation pathways

Seenivasan Laskhmi Prabavathi [a], Karunamoorthy Saravanakumar [b], Chang Min Park [b], Velluchamy Muthuraj [a],*

[a] Department of Chemistry, V. H. N. Senthikumara Nadar College (Autonomous), Virudhunagar 626 001, Tamil Nadu, India
[b] Department of Environmental Engineering, Kyungpook National University, 80 Daehak-ro, Buk-gu, Daegu 41566, Republic of Korea

ABSTRACT

Recent year pharmaceutical pollutants have highly detected in environment, because they do not completely mineralized and remain toxic. Semiconductor photocatalyst materials have well recognized as promising technology for environmental pollutants removal in the presence of visible light. In this work, a novel binary Sm_6WO_{12} modified g-C_3N_4 nanosheets heterojunction was fabricated *via* simple facile method. The morphology of the newly prepared g-C_3N_4 and Sm_6WO_{12} was confirmed as nanosheets and nanorods by using microscopy techniques. The sequence of characterization results verified that the Sm_6WO_{12}/g-C_3N_4 synergistically integrate the excellent properties and successful construction of hetero-structure between the Sm_6WO_{12} and g-C_3N_4. The Sm_6WO_{12}/g-C_3N_4 nanocomposite heterojunction catalyst shows higher photocatalytic efficiency towards degrading pharmaceutical pollutant levofloxacin compared to individual g-C_3N_4 and Sm_6WO_{12} photocatalyst. The results indicate that about 90.8% of levofloxacin was degraded after 70 min in the presence of Sm_6WO_{12}/g-C_3N_4 nanocomposite. Through radical trapping experiments, $O_2^{\bullet-}$ and $^{\bullet}OH$ were proved to be the leading reactive oxidative species contributing to degradation of levofloxacin. Possible photodegradation pathways were proposed based on the detected intermediate products and transformation products. Furthermore, the synthesized Sm_6WO_{12}/g-C_3N_4 heterojunction demonstrated excellent reusability and stability without of loss of photocatalytic activity. Favorably, this study might provide a deep insight into mechanism and possible degradation pathways of levofloxacin by Sm_6WO_{12} modified g-C_3N_4 heterojunction photocatalyst.

1. Introduction

Levofloxacin is a well-known synthetic fluoroquinlone antibiotic, which has been widely used in treatment of severe or life-threatening bacterial infections. Levofloxacin is not completely metabolized (only 15–20%) in human and animal bodies, due to their chemical structure and released as pharmaceutically active forms through the environment *via* human and animal feces and urine [1,2]. The presences of levofloxacin in environment at above relevant levels produce the chronic toxic effect and serious threat to human health and living organism. A variety of physical, chemical and biological post and pre-treatment technique were used to eliminate the pollutants present in the environment [3,4].

In the past decades, photocatalytic technology is one of most important technology for researcher. This technology was limited to application in harvesting solar energy, but it also useful in numerous environmental applications, particularly wastewater treatment [5,6]. The mechanism involves the photocatalysis is absorption of photon light energy by the catalyst. The organic pollutants can simply degraded *via* the highly active hole (h^+) or the excited electron producing highly reactive radicals. In most of the photocatalyst, the excited electron and h^+ undergo recombination leading to reduced photocatalytic efficiency. Various metal-containing and metal-free semiconductors photocatalyst were discovered in recent years [7–10]. Metal free graphitic carbon nitride (g-C_3N_4) have drawn a great interest due to its facile and economic synthesis, suitable band gap for harvesting solar energy, thermal stability, reliable chemical inertness, in addition to electrochemical, versatile and well-organized photocatalytic properties [11–13]. Its narrowing band gap and strong visible light absorbing ability make it perform well in photocatalysis. Nonetheless, the fast recombination rate of charge carriers (electron-hole pairs) and poor conductivity which largely limits the activity in the practical applications.

To address, many attempts such as element-doping, nano-structuring, composite constructing and so on are useful approaches to develop the superior catalyst for the organic pollutants degradation [14,15]. Elemental doping and composite constructing are essentially alter the electronic and structural properties of g-C$_3$N$_4$, nano-structuring mainly increase the specific surface area of g-C$_3$N$_4$ [16]. In common, different approach contributes in different way to increase the certain properties of g-C$_3$N$_4$ catalyst. Among these strategies, constructing a composite could bring preservative effect to promote electron-hole pairs separation and develop into new trend in the design of advance photo-catalyst [17–19]. Considering merits of composite constructing, most composites associated with g-C$_3$N$_4$ had been reported, such as g-C$_3$N$_4$/CdWO$_4$, Sn$_3$O$_4$/g-C$_3$N$_4$, g-C$_3$N$_4$/CdS, and CuInS$_2$/g-C$_3$N$_4$ subsequently [20–23]. This approach is known to retard the charge carrier's recombination process.

Recent years, rare earth metal tungstates materials have attracted great interest for many researchers due to their potential application and excellent properties such as high oxide ion conductivity, high thermal and chemical stability, and good mechanical property [24,25]. As a kind of rare-earth metal tungstate, samarium tungstate has been found to present excellent performance in luminescence, conductor in fuel solid oxide and anode materials and photocatalyst [26,27]. Due to the more negative conduction band position of samarium tungstate, it's coupling with g-C$_3$N$_4$ will make available a proper way to accepting the electrons of g-C$_3$N$_4$ thereby enhancing its activity more efficiently. Therefore, the samarium tungstate doped g-C$_3$N$_4$ heterojunction has excellent performance and could be more practical for environmental application.

In this study, we demonstrated to design a novel Sm$_6$WO$_{12}$ decorated g-C$_3$N$_4$ heterojunction for degradation of levofloxacin from aqueous phase. The as-synthesized photocatalyst structural properties and morphology was investigated in detail in terms of various spectroscopic and analytical techniques such as XRD, XPS, FT-IR, UV–vis DRS, PL, SEM, EDX, TEM and BET analysis. The effect of initial concentration and catalyst dosages were systematically explored in detail. The main reactive radical species in the degradation process determined by scavenger study. Based on the identified intermediates by GC–MS, the photocatalytic degradation pathways also been proposed.

2. Experimental sections

2.1. Materials

Melamine (C$_3$H$_6$N$_6$, 99%), sodium tungstate dihydrate (Na$_2$WO$_4$·2H$_2$O, 99%) and samarium nitrate (Sm(NO$_3$)$_3$, 99.9%), ethyl alcohol (C$_2$H$_5$OH, 95%), benzoquinone (BQ, C$_6$H$_4$O$_2$, 98%), ammonium oxalate ((NH$_4$)$_2$C$_2$O$_4$, 99%), *tert*-butyl alcohol (TBA, C$_4$H$_{10}$O, 99%), levofloxacin (C$_{18}$H$_{20}$FN$_3$O$_4$, 98%) were analytical grade and used without further purification which purchased from Merck, India. Deionized water and double distilled water used to throughout the work.

2.2. Preparation of polymeric g-C$_3$N$_4$

g-C$_3$N$_4$ was prepared through the direct heating of melamine (10 g) in a muffle furnace at 550 °C for 4 h. After reaction, the lid closed crucible was cooled to atmospheric temperature and the resulting yellow g-C$_3$N$_4$ powder was collected for further use.

2.3. Preparation of Sm$_6$WO$_{12}$

Sm$_6$WO$_{12}$ was fabricated by one pot single step hydrothermal strategy using Na$_2$WO$_4$·2H$_2$O and Sm(NO$_3$)$_3$ as the precursor. Sm(NO$_3$)$_3$ (1.33 g) and Na$_2$WO$_4$·2H$_2$O (1 g) each were dissolved separately in 15 mL of deionized water in 100 mL beaker and stirred for 3 h and mixed together. The resultant solution was transfer into stainless steel autoclave with capacity of 100 mL and heated in a muffle furnace at 180 °C for 12 h. The resulting precipitate washed with water and absolute
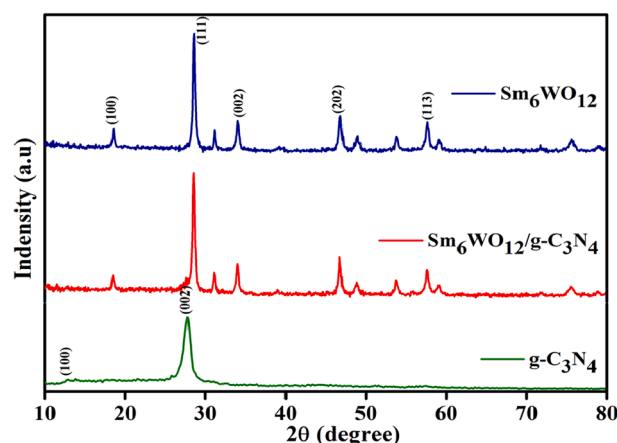

Fig. 1. XRD patterns of pure g-C$_3$N$_4$, pristine Sm$_6$WO$_{12}$ and Sm$_6$WO$_{12}$/g-C$_3$N$_4$ heterojunction.

ethanol for several times and then allowed dry at 60 °C for 16 h in a vacuum oven. The obtained hydrothermally reacted product was calcination at 800 °C in air atmosphere.

2.4. Preparation of Sm$_6$WO$_{12}$/g-C$_3$N$_4$

The Sm$_6$WO$_{12}$/g-C$_3$N$_4$ hetero-structure photocatalyst was fabricated by using the following procedure. The equal weight ratio of Sm$_6$WO$_{12}$ and g-C$_3$N$_4$ was added in a mortar and ground for mixing. The resulting mixture was added into 30 mL of absolute ethanol under ultrasonication for 10 min to form uniform suspension. The obtained sample was filtered and washed with ethanol and then dried. Finally, the obtained sample was grounded and calcined at 500 °C for 2 h [28,29].

2.5. Physicochemical characterization

The crystal structure of the sample were obtained on PANalytic X'Pert Pro X-ray diffraction measuring with Cu Kα in the range of 2θ (10–80°). The element chemical oxidation states and valence information of the as prepared samples were analyzed by (Multi-Lab 2000, Thermo Scientific) X-ray photoelectron spectroscopy and the optical properties were determined by UV–vis diffuse reflection spectrum (Shimadzu-2450, Japan) spectrophotometer. Fourier Transform Infrared spectrum were carried out by (Perkin-Elmer 783, USA) using KBr as internal reference and accelerating voltage range was 4000–400 cm^{-1}. The structure and morphology of the synthesized samples were recorded using a scanning electron microscopy (SEM, Carl Zeiss EVO 18, Germany) and transmission electron microscopy (JEOL JEM 2100, Japan). The specific surface area were carried out by using liquid N$_2$ adsorption–desorption equilibrium at 77 K by (Micromeritics ASAP 2020, USA) Porosimeter. The transient photocurrents and electrochemical impedances spectroscopy (EIS) measurements were conducted by electrochemical analyzer (CHI660A, CH instrument Co, USA) in a slandered three electrodes system. The photocatalytic intermediates products were identified by (Perkin Elmer Clarus 500, USA) GC–MS. The prepared samples charge carrier's properties were analyzed with fluorescence spectrometer (Shimadzu F-4000, Japan) at room temperature and the excited wavelength was 470 nm.

2.6. Measurements of photocatalytic tests

The photocatalytic abilities of as synthesized Sm$_6$WO$_{12}$/g-C$_3$N$_4$ heterojunction were evaluated by the photodegradation removal of levofloxacin under visible light illumination. In this experiment, 50 mg of the catalyst was added into a 100 mL of levofloxacin (10 mg/L) solution. Prior irradiation, the above suspension was allowed stir for 30
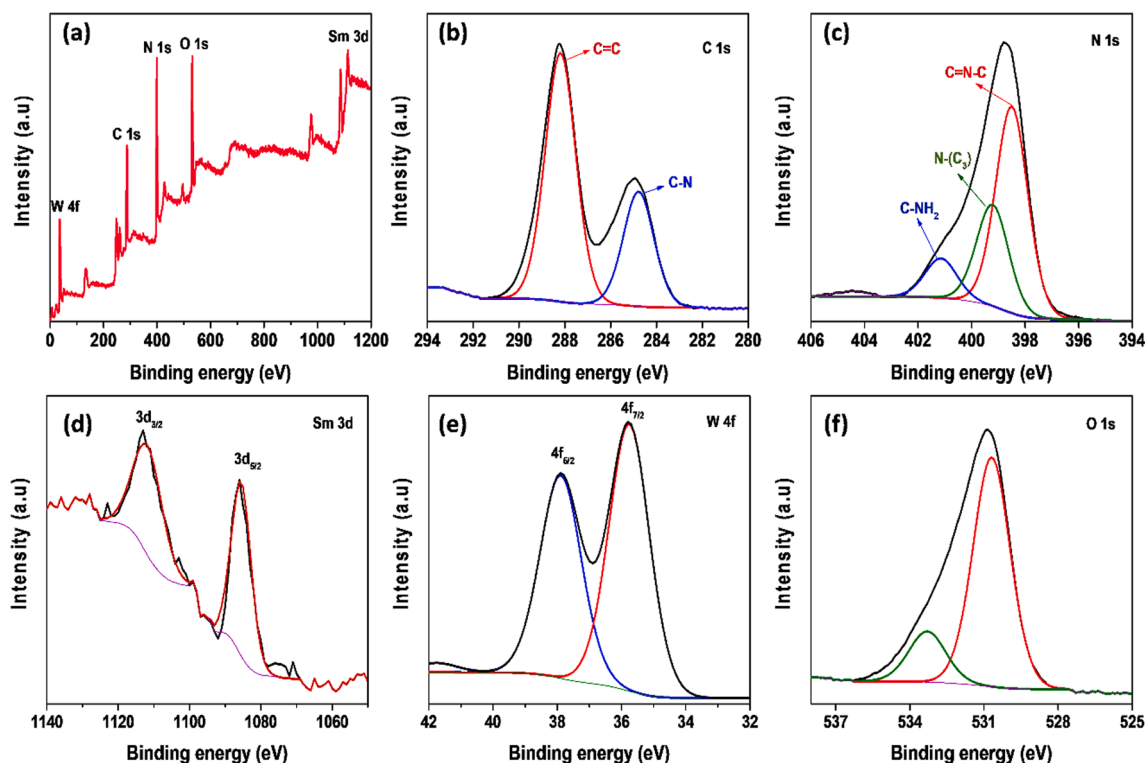
Fig. 2. XPS spectra of $Sm_6WO_{12}/g\text{-}C_3N_4$ heterojunction: (a) survey spectrum, (b) C 1s, (c) N 1s, (d) Sm 3d, (e) W 4f, and (f) O 1s.

min in dark medium to attain the equilibrium between photocatalyst and pollutant. Then, the resulting solution (catalyst + pollutant) was bared to a 150 mW/cm^{-2} tungsten lamp (visible light source). During the reactions, 3 mL of aliquot was collected by filtration every 10 min and measured the characteristic main absorption peak (λ = 287 nm) using UV–vis spectrophotometer.

3. Results and discussion

3.1. XRD and FT-IR analysis

The pristine g-C$_3$N$_4$, pure Sm$_6$WO$_{12}$, and Sm$_6$WO$_{12}$/g-C$_3$N$_4$ nanocomposite crystalline structure were investigated through X-ray diffraction (XRD), which demonstrated in Fig. 1. From the Fig. 1, the pure Sm$_6$WO$_{12}$ has tetragonal structure and high crystalline in nature, and it is well consistent with standard data (JPDS card No. 22-1308). The bare Sm$_6$WO$_{12}$ exhibits the diffraction peaks at 2θ = 18.45°, 28.49°, 33.98°, 46.48° and 57.6° are assigned to the (1 0 0), (1 1 1), (0 0 2), (2 0 2) and (1 1 3) planes respectively. For pure g-C$_3$N$_4$, there are two bragg's diffractions at 12.85 and 27.81°, matching to the (1 0 0) and (0 0 2) diffraction crystal planes, respectively. The diffraction peak at 12.85° was ascribed to the in-plane repeat period of tri-s-triazine units and the peak at 27.81° is assigned to the stacking of conjugated aromatic compound [30]. Nonetheless, the peak (0 0 2) of g-C$_3$N$_4$ has not visible in Sm$_6$WO$_{12}$/g-C$_3$N$_4$ heterojunction, maybe due to the overlapping of (1 1 1) diffraction peak of Sm$_6$WO$_{12}$ and g-C$_3$N$_4$ peak of (0 0 2), and the peak intensity was also increased, which is due to FWHM value decreased. Debye-Scherrer's equation (χ = kλ/βcosθ) was used to find out the crystalline size of Sm$_6$WO$_{12}$ and Sm$_6$WO$_{12}$/g-C$_3$N$_4$ heterojunction using (1 1 1) plane [31,32]. The crystalline size of Sm$_6$WO$_{12}$ is 33.24 nm and Sm$_6$WO$_{12}$/g-C$_3$N$_4$ heterojunction is 27.68 nm, respectively.

Fig. S1 illustrates the FTIR absorption spectra of bare g-C$_3$N$_4$, pure Sm$_6$WO$_{12}$ and Sm$_6$WO$_{12}$/g-C$_3$N$_4$ nanocomposite, which investigate the functional group of the composite. The characteristic peaks at 1245 and 1410 cm^{-1} were observed as the stretching vibration of heterocyclic

C—N functional group. The sharp absorption peak at 811 cm^{-1} is assigned to the tri-s-triazine units based on stretching vibration mode. The broad bands at 1321 and 1666 cm^{-1} are correspond to the vibration modes of C—N and C=N, respectively [33–35]. For the bare Sm$_6$WO$_{12}$ sample, the stretching of the Sm—O—Sm bond was examined a peak at 541 cm^{-1}. The absorption peak at 857 cm^{-1} was corresponding to the asymmetric vibration of the metal–oxygen (W—O) bond [36]. Most of the characteristic absorption peaks of pure g-C$_3$N$_4$ and Sm$_6$WO$_{12}$ all exist in the Sm$_6$WO$_{12}$/g-C$_3$N$_4$ nanocomposite.

3.2. Surface chemical properties

Sm$_6$WO$_{12}$/g-C$_3$N$_4$ heterojunction, pure Sm$_6$WO$_{12}$ and pristine g-C$_3$N$_4$ samples surface composition and chemical states were investigated by XPS, it revealed in Fig. 2. The XPS survey spectrum of Fig. 2a suggests that C, N, Sm, W and O elements exist in Sm$_6$WO$_{12}$/g-C$_3$N$_4$ heterojunction. In C 1s high resolution spectrum shows two peaks located at 284.9 and 288.2 eV, were attributed to the sp^2 hybridized graphitic carbon (C—C or C=C) bonds and sp^3 bonded C in N$_2$—C=N, respectively (Fig. 2b). The N 1s spectrum Fig. 2c, the three strong peaks at 398.7, 399.4 and 401.1 eV corresponding to the sp^2 hybridized aromatic N (C—N=C) groups, tertiary N bonded C atoms (N—C$_3$), and NH$_2$ functional groups with an H atom (C—NH$_2$), respectively [37]. From Fig. 2d, the Sm 3d high-resolution spectrum reveals that, the two peaks at 1085.6 and 1112.1 eV was allocated to Sm 3d$_{5/2}$ and Sm 3d$_{3/2}$ corresponding the presence of Sm^{3+} state in Sm$_6$WO$_{12}$. Fig. 2e shows the high resolution spectrum of W 4f, where the binding energies at 35.76 and 37.93 eV correspond to the W 4f$_{7/2}$ and W 4f$_{5/2}$ peaks for Sm$_6$WO$_{12}$, corresponding to W^{6+} valance state. In the O 1s spectrum (Fig. 2f), the peak at 530.5 eV for O^{2-} was attributed to the lattice oxygen atom of Sm$_6$WO$_{12}$. The peak appeared at 531.9 eV was attributed to the existence of hydroxyl group (O—H) or surface water molecules.

3.3. Morphological, textural and thermal properties

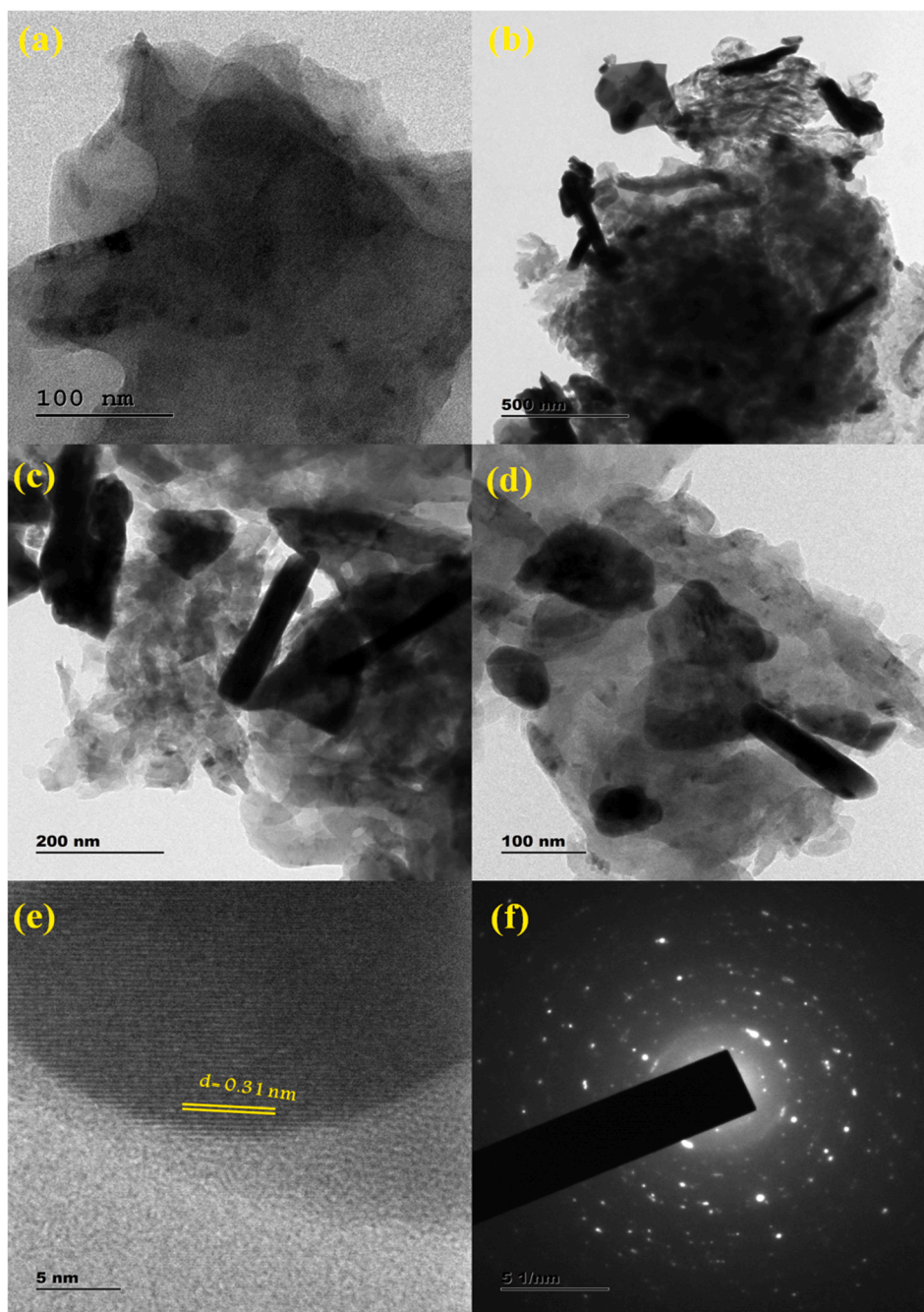To investigate the topographical features and morphological of the as

Fig. 3. TEM images of (a) pure g-C$_3$N$_4$, (b-d) Sm$_6$WO$_{12}$/g-C$_3$N$_4$ heterojunction with different magnification. (e) HRTEM images of Sm$_6$WO$_{12}$/g-C$_3$N$_4$ heterojunction and (f) corresponding SAED pattern.

prepared samples, SEM and TEM were executed. SEM micro images of Sm$_6$WO$_{12}$, pristine g-C$_3$N$_4$ and Sm$_6$WO$_{12}$/g-C$_3$N$_4$ heterojunction were displayed in Fig. S2. Fig. S2a reveals that the g-C$_3$N$_4$ exhibits the comprehensive layer structure with stacking of several layers. The pure Sm$_6$WO$_{12}$ demonstrated that rods like structure with agglomerated particles and smooth surface (Fig. S2b). However, the Sm$_6$WO$_{12}$/g-C$_3$N$_4$ heterojunction surface morphology was composed of a rod like structure of Sm$_6$WO$_{12}$ highly anchored on the surface of g-C$_3$N$_4$ (Fig. S2c). Additionally, the EDX spectrum of Sm$_6$WO$_{12}$/g-C$_3$N$_4$ heterojunction was displayed in Fig. S2d. It is noteworthy that the heterojunction contains only C, N, O, Sm, W and O elements, the result demonstrate the formation of Sm$_6$WO$_{12}$ and bare g-C$_3$N$_4$.

The detailed morphology of the samples were recorded by TEM, which displayed in Fig. 3. The pristine g-C$_3$N$_4$ morphology was appeared

as sheet like structure and the sheet thickness is several nanometers (Fig. 3a). Fig. 3(b–d) can be clearly observed that the Sm$_6$WO$_{12}$ nanorods are randomly anchored on the g-C$_3$N$_4$ surface and some irregular shapes of Sm$_6$WO$_{12}$ were also presented on g-C$_3$N$_4$. Meanwhile, clear lattice fringes with interlayer distance of 0.31 nm corresponding to (1 1 1) plane of Sm$_6$WO$_{12}$ nanorods were observed from HR-TEM image and its good consists with XRD results (Fig. 3e). Fig. 3f shows the, SAED pattern of Sm$_6$WO$_{12}$/g-C$_3$N$_4$ heterojunction, the presence of concentric diffraction rings, indicating that the dispersed Sm$_6$WO$_{12}$ nanocomposite was polycrystalline.

The specific surface area of the pristine g-C$_3$N$_4$ and Sm$_6$WO$_{12}$/g-C$_3$N$_4$ sample was analyzed by using liquid nitrogen (N$_2$) adsorption–desorption equilibrium conditions were displayed in Fig. 4. Generally, the large surface area photocatalyst has improved the charge
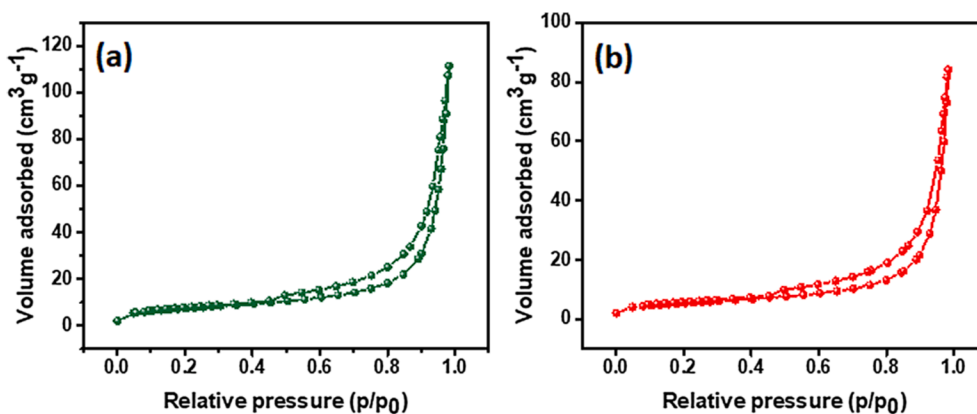
Fig. 4. N_2 adsorption–desorption isotherms of (a) g-C_3N_4 and (b) Sm_6WO_{12}/g-C_3N_4 nanocomposite.
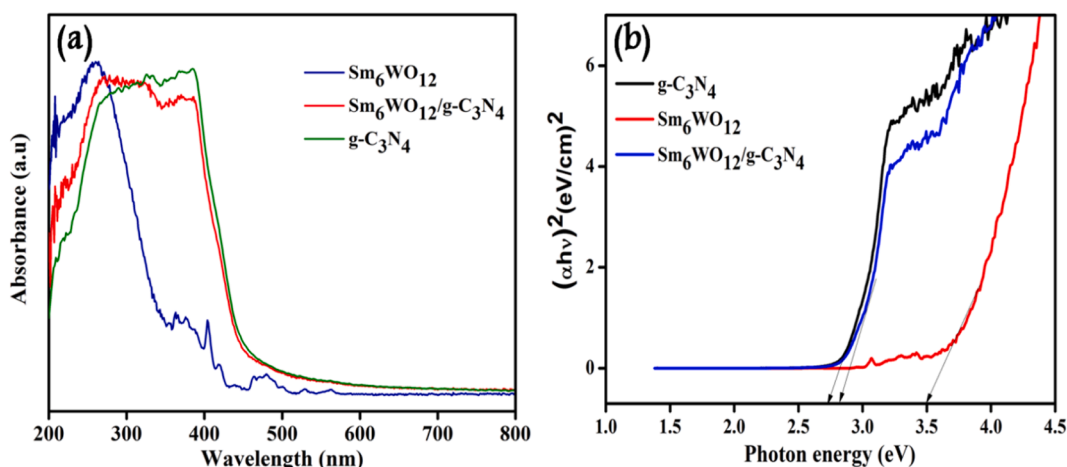

Fig. 5. (a) UV–*vis* DRS and (b) Tauc's plot of g-C_3N_4, Sm_6WO_{12}, and Sm_6WO_{12}/g-C_3N_4 heterojunction.

separation that leads to the enhanced photocatalytic activity with higher reactive active sites. The specific surface area of bare g-C_3N_4 and Sm_6WO_{12}/g-C_3N_4 nanocomposite was 24.1 and 17.8 m^2g^{-1}, respectively. The specific surface area of Sm_6WO_{12}/g-C_3N_4 nanocomposite was less than that of bare g-C_3N_4, suggesting that Sm_6WO_{12}/g-C_3N_4 nanocomposite was decorated on the g-C_3N_4 surfaces or pores were blocked.

The thermal stability of the synthesized materials was examined by Thermogravimetric analysis (TGA-DSC measurements). The thermogram (Fig. S3a) of pure g-C_3N_4 exhibited a sharp weight loss in the range of 530–600 °C. Further increasing heating temperature caused the decomposition of g-C_3N_4, chemically converting carbon nitride into carbon and nitrogen containing gases. As can be seen from Fig. S3b, the decomposition of Sm_6WO_{12}/g-C_3N_4 nanocomposite started at 630 °C. At 700 °C, a sharp weight loss was observed due to the complete degradation of Sm_6WO_{12} doped g-C_3N_4 sheets. The DSC curve shows an exothermal peak, which is due to the decomposition of g-C_3N_4. Moreover, the TGA measurement shows that the decomposition temperature of Sm_6WO_{12}/g-C_3N_4 composites was lower than the pristine g-C_3N_4. The shift of weight loss towards lower temperature was considered due to some changes in surface chemistry of the g-C_3N_4 during forming of heterojunction structure with other materials.

3.4. Optical properties

The photo-absorption behavior of the as-synthesized binary nanocomposite as well as bare g-C_3N_4 and Sm_6WO_{12} were exemplified by utilizing UV–vis DRS. Fig. 5a shows the pure g-C_3N_4 observed the strong absorption edge at 300 nm to 460 nm which correlates with the intrinsic

band gap energy (2.7 eV). Contrasted with pristine g-C_3N_4, the edge of absorption of Sm_6WO_{12}/g-C_3N_4 heterojunction reveals distinct blue-shift, which can originate from the Sm_6WO_{12} nanorods are decorated on the g-C_3N_4 nanosheets. This blue shift absorption results from increase the energy gap of Sm_6WO_{12}/g-C_3N_4 nanocomposite. Additionally, the energy gap values of the as-synthesized catalysts was confirmed by using Tauc's equation as displayed in Fig. 5b. Tauc's relation was described given below [38]:

$$\alpha \ = \ C/h\nu(h\nu - Eg)^{-1/2} \tag{1}$$

where α is the light absorption coefficient semiconductor, ν is frequency, Eg is average energy gap, h is Planck's constant and C is proportional constant. Based on Fig. 5b, the band gap of g-C_3N_4, Sm_6WO_{12} and Sm_6WO_{12}/g-C_3N_4 hetero-structure was observed approximately 2.72, 3.5 and 2.81 eV respectively. The increased band gap of Sm_6WO_{12}/g-C_3N_4 heterojunction compared to g-C_3N_4 due to the quantum confinement effect [39,40].

Photogenerated e^- and h^+ pair recombination is a vital factor, which is affecting the photocatalytic reaction rate of the materials. The main disadvantage of g-C_3N_4 was rapid recombination rate of e^- and h^+ pairs, this problem was reduced due to the formation of heterojunction. The PL spectrum was used to verify the effect of heterojunctions on the diminution of the photogenerated charge carrier's recombination rate. The PL spectrum of singe g-C_3N_4, Sm_6WO_{12} and Sm_6WO_{12}/g-C_3N_4 hetero-structure were displayed in Fig. S4. As for g-C_3N_4, the PL peak intensity was relatively high, which designated that rapid recombination of photoexcited e^- and h^+ pairs. While the combined with Sm_6WO_{12}, the
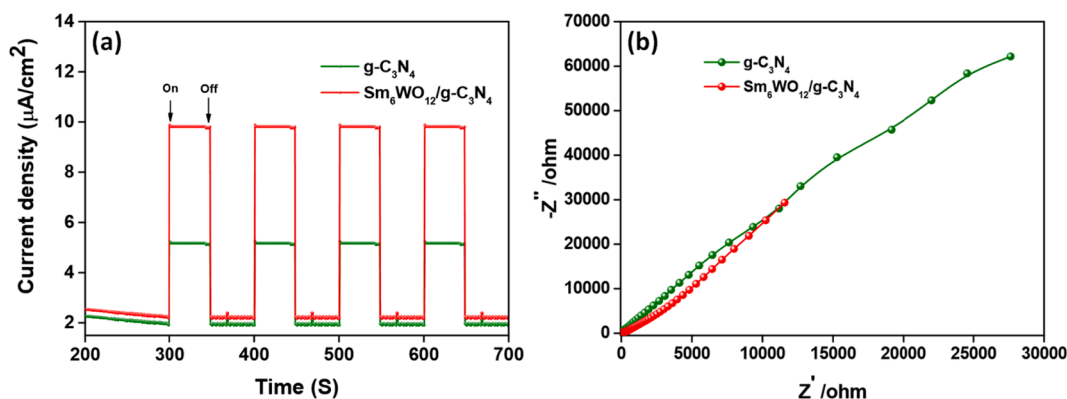
Fig. 6. (a) Transient photocurrent response curves and (b) the corresponding electrochemical impedance (EIS) spectra of g-C_3N_4, and Sm_6WO_{12}/g-C_3N_4 heterojunction.
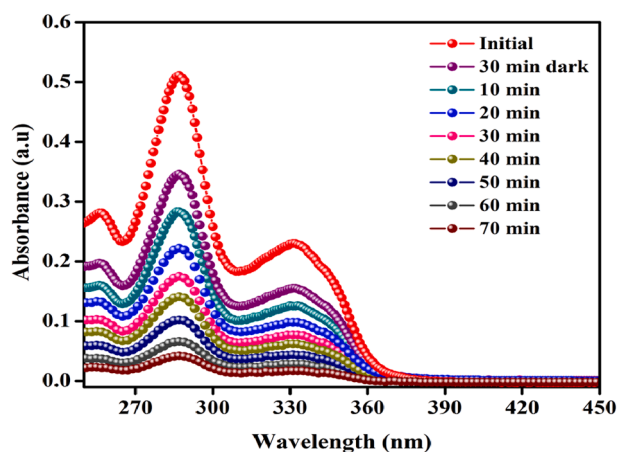
Fig. 7. Absorption spectra for degradation of levofloxacin over Sm_6WO_{12}/g-C_3N_4 heterojunction.

Sm_6WO_{12}/g-C_3N_4 PL peak intensity was decreased, it suggests that the Sm_6WO_{12}/g-C_3N_4 heterojunction can be efficiently quenched the recombination behavior of e^--h^+ pairs.

To study the separation and transfer efficiency of charge carriers (electron-hole) generated in the nanocomposites, the photocurrent response is obtained after four on–off cycles of visible light irradiation. The photogenerated electron-hole charge separation and transfer performance were investigated by a combined analysis of photocurrent responses and electrochemical impedance spectroscopy (EIS). As shown in Fig. 6a, Sm_6WO_{12}/g-C_3N_4 heterojunction exhibits an improved photocurrent responses compared to pure g-C_3N_4, indicating that the hinder the recombination of photogenerated carriers and more efficient transport of electrons [4]. From the Fig. 6b, compared with the pure g-C_3N_4 and Sm_6WO_{12}/g-C_3N_4 heterojunction has the smaller arc radius on EIS Nyquist plot which further manifests the separation and transfer efficiency of photogenerated carriers. This results are good consistent with the PL test results [41]. The higher photocurrent density and smaller arc radius confirm the effective separation rate of the photogenerated electron–hole pairs in the Sm_6WO_{12}/g-C_3N_4 heterojunction.

3.5. Photocatalytic activity

Fig. 7 displays the UV–vis absorption spectra for the photodegradation of levofloxacin in the presence of Sm_6WO_{12}/g-C_3N_4 heterojunction photocatalyst. It can be noted that the absorbance peak of levofloxacin at 287 nm steadily decreased with increase of the light irradiation time without any shifts. The photocatalytic reaction

properties of all catalyst were carried out by degradation of levofloxacin over visible light illumination and the result are demonstrated in Fig. S5a. As obvious, the pure Sm_6WO_{12} photocatalyst has weaker photocatalytic activity for degradation of levofloxacin after 70 min. However, 10.96% levofloxacin was degraded in the presence of pure Sm_6WO_{12} within same duration. In contrast, the degradation of levofloxacin (90.8%) was enriched after the loading of Sm_6WO_{12} on g-C_3N_4. The Sm_6WO_{12}/g-C_3N_4 heterojunction revealed superior photocatalytic performance than that of individual component, which can be effectively transfer and retard the charge carriers (e^--h^+ pairs).

To quantitatively study the reaction kinetics of the levofloxacin degradation over Sm_6WO_{12}/g-C_3N_4 heterojunction, the photocatalysis experiment data followed the first order kinetics with respect to the rate constant (k) and the concentration of levofloxacin can be calculated from the following Eqs:

$$ln(C_t/C_0) = k_{app}t \tag{2}$$

where k_{app} (min^{-1}) is apparent rate constant, C_0 (mg/L) and C_t (mg/L) are the initial and final levofloxacin concentration, t (min) is the irradiation time of the experiment. From the Fig. S5b displays that, the photocatalytic degradation of levofloxacin experimental data was follows first order reaction dynamics over our experimental reaction conditions. The calculated rate constant (k) value of pure g-C_3N_4, pristine Sm_6WO_{12} and Sm_6WO_{12}/g-C_3N_4 heterojunction was 0.0116, 0.1161 and 0.034 min^{-1}, respectively. Noticeably, the Sm_6WO_{12}/g-C_3N_4 have highest photocatalytic degradation rate constant, which was up to 20.52 and 2.93 times higher as that of single Sm_6WO_{12} and pure g-C_3N_4, respectively. Thus the above discussion clearly indicates that the loading of Sm_6WO_{12} nanomaterials on g-C_3N_4 nanosheets could be strongly motivated the photocatalytic efficiency, owing to its retard the charge carriers (e^--h^+ pairs).

Influence of initial concentration of levofloxacin and photocatalyst dosage on levofloxacin degradation was investigated, which displayed in Fig. S6. Fig. S6a shows the plot of C/C_0 *vs* irradiation time in the presence of photocatalyst of Sm_6WO_{12}/g-C_3N_4 by varying catalyst dosage 10–70 mg. The degradation rate of levofloxacin by varying catalyst dosage was found to be 64.1% (10 mg), 71.3% (30 mg), 75.9% (70 mg) and 90.8% (50 mg) respectively. Maximum degradation efficiency was achieved when loading of photocatalyst dosage at 50 mg, due to increase the density of active sites of Sm_6WO_{12}/g-C_3N_4 heterojunction photocatalyst. As the amount of Sm_6WO_{12}/g-C_3N_4 heterojunction dosage was further increased 70 mg, the number of active site increased for reactions but the light penetration was decreased by the excess amount of catalyst. The above discussion indicates that the optimal Sm_6WO_{12}/g-C_3N_4 catalyst dosage was 50 mg for the photocatalytic reaction [41,42]. Fig. S6b illustrates the degradation removal of levofloxacin in different initial concentration of levofloxacin aqueous
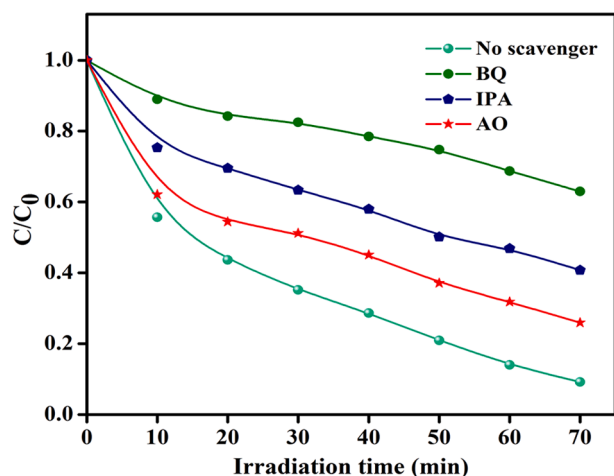
Fig. 8. Reactive species trapping experiment of Sm_6WO_{12}/g-C_3N_4 with levofloxacin under visible light.

solution in the presence of catalyst. The observed photodegradation activity was high at lower concentration of drug (10 mg/L) and lower efficiency at high concentration of drug (30 mg/L) under visible light illumination. The photocatalytic efficiency was decreased at high concentration may be due to the lesser formation of oxidants and active site on the photocatalyst covered by levofloxacin. It can be reducing the light penetration and consequently the production active radical species generation also decreased at high concentration [43].

The stability of photocatalyst was determined to conduct recyclability test, as it is significant from application point of view. The photocatalyst was recuperated by centrifugation after it's utilize in the photodegradation experiments and washed with D.I water and absolute ethanol for more than a two time to eradicate the unwanted materials. The recovered catalyst was dried at 80 °C for overnight and then used for consequent experiments. Fig. S7a shows the photodegradation of levofloxacin for five successive runs. After five cycles, the photodegradation efficiency of the catalyst was decreased slightly as compared to the first cycle. In this result indicated that, Sm_6WO_{12}/g-C_3N_4 heterojunction

possessed higher stability and recyclability. Fig. S7b, the XRD pattern shows the crystal and phase structure of Sm_6WO_{12}/g-C_3N_4 catalyst do not change the before and after reusability test.

3.6. Proposed removal mechanisms of levofloxacin by the composite

To evaluate the photodegradation mechanism, the effects of various reactive oxidative species (ROS) on the degradation of levofloxacin over Sm_6WO_{12}/g -C_3N_4 were determined in Fig. 8. In this photocatalytic study, isopropyl alcohol (IPA), benzoquinone (BQ), and ammonium oxalate (AO), were employed to the capture of hydroxyl radical ($^\bullet OH$), superoxide ($O_2^{\bullet -}$) and holes (h^+) reactive species in photocatalyst process, respectively. The degradation efficiency of levofloxacin was obviously quenched after addition of BQ and IPA into the system, which demonstrated that $O_2^{\bullet -}$ and $^\bullet OH$ radicals were played predominant role in the photodegradation process. Moreover, the addition of trapping agent of AO into the photocatalytic system can also the degradation efficiency was of levofloxacin decreased, suggesting that the h^+ was slightly influence on the photodegradation of levofloxacin [44,45].

The enriched the photocatalytic performance of Sm_6WO_{12}/g-C_3N_4 which mainly ascribed to its synergistic interactions of g-C_3N_4 and Sm_6WO_{12} which encourages the effective separation of charge carriers (e^--h^+ pairs). Based on the above result and discussions, a possible photo degradation mechanism of levofloxacin over Sm_6WO_{12}/g-C_3N_4 heterojunction has been proposed in Fig. 9. The CB and VB edge potential of semiconductor photocatalyst were determined by using the Mulliken electronegativity theory [46,47],

$$E_{CB} = \chi - E_e - 0.5\ Eg \qquad (3)$$

$$E_{VB} = E_{CB} + Eg \qquad (4)$$

where Eg is band gap energy of semiconductor, χ is electronegativity and E_e is the free electrons of the energy on the standard hydrogen spectrum (~4.5 eV). The Sm_6WO_{12}/g-C_3N_4 nanocomposite can easily absorb the photon energy to generate prosperity of electrons and holes in its CB and VB. The photoexcited electrons quickly transfer to the Sm_6WO_{12} (CB = −1.0982 eV) nanocomposite due to the CB band edge potential of g-C_3N_4 (CB = −1.148 eV) which was more negative potential. Moreover, the accumulated electron in the CB of Sm_6WO_{12} could use oxygen (O_2)
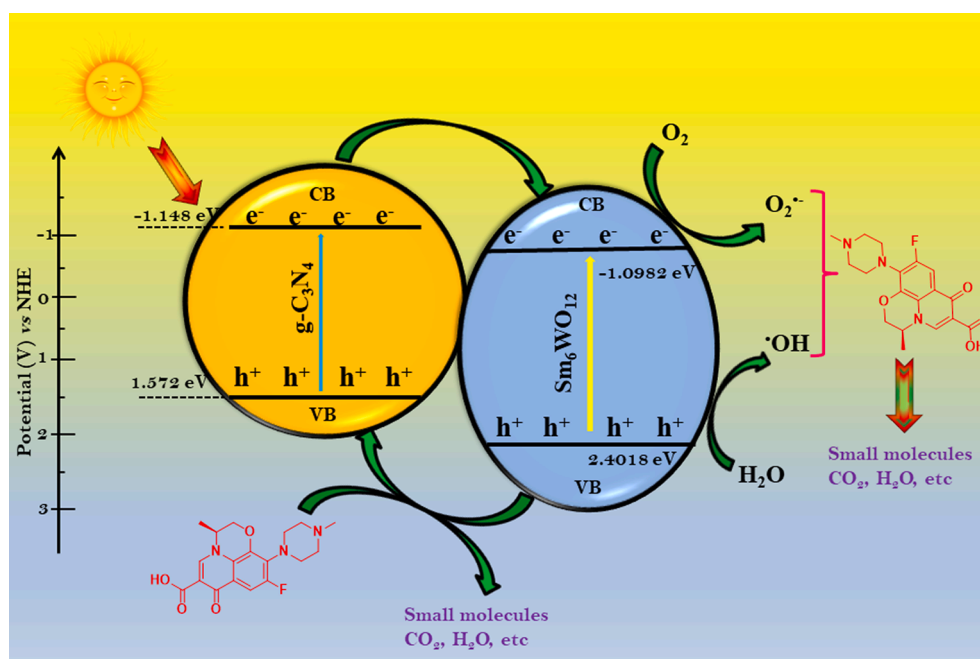

Fig. 9. Photocatalytic mechanism of levofloxacin over Sm_6WO_{12}/g-C_3N_4 heterojunction.

Table 1

Comparison of Levofloxacin degradation by various nanocomposites under visible light irradiation.

Catalysts	Pollutants	Conc. (mg/L)	Time (min)	Activity (%)	Ref
Ag/AgBr/ BiOBr	Levofloxacin	10	90	74	[44]
CdS	Acetaminophen, Levofloxacin	5	240	85, 70	[50]
Bi$_2$WO$_6$	Levofloxacin	10	150	80	[45]
TiO$_2$	Levofloxacin	25	120	90	[51]
Ag$_2$O/TiO$_2$	Levofloxacin	10	90	81	[52]
CeVO$_4$- BiVO$_4$	Levofloxacin	50	300	95.7	[53]
Sm$_6$WO$_{12}$/ g-C$_3$N$_4$	Levofloxacin	10	70	90.8	This study

molecules to generating O$_2^{\bullet-}$ radicals, because their CB were greater than 0.33 eV. Furthermore, the O$_2^{\bullet-}$ oxidizes levofloxacin to produce degradation product. The photoinduced h$^+$ on the VB of Sm$_6$WO$_{12}$ can transfer easily to g-C$_3$N$_4$ because the VB potential of Sm$_6$WO$_{12}$ (VB = 2.4018 eV) more positive potentials than g-C$_3$N$_4$ (VB = 1.572 eV). The h$^+$ are scavenger by H$_2$O or hydroxyl ions (OH$^-$) to generate $^{\bullet}$OH, producing $^{\bullet}$OH to oxidize levofloxacin and effectively enhance the phtotocatalytic performance of Sm$_6$WO$_{12}$/g-C$_3$N$_4$. The as synthesized Sm$_6$WO$_{12}$/g-C$_3$N$_4$ heterojunction photocatalytic efficiency was compared with other photocatalyst reported in literature [50–53] as tabulated in Table 1.

An intermediate product of the photocatalytic reaction was identified by GC–MS. The important intermediate steps of levofloxacin degradation as shown in Fig. 10. The chromatograms of the identified main photodegradation products as shown in Fig. S8. They were used to understand various degradation mechanism of mineralization product in levofloxacin. During this degradation process of levofloxacin was initially produced an intermediates compounds was formed were based on molecular ion peaks M + 1 (L, $m/z = 363.16$). According to this molecular ion peak undergoes decarboxylation reaction of methyl-morpholine group in levofloxacin drug was transform in to L2, ($m/z = 335.16$) [43]. The important intermediate of levofloxacin at $m/z = 279$ (L2) was further degradation occurs on N-methyl piperazine ring, it was oxidized and stable intermediate to form ($m/z = 380.12$) L3 [48]. Afterwards intermediates compound L3 was further de-alkylation to produce two intermediate such as $m/z = 266.11$ (L4) and $m/z = 252.09$ (L5), this L4 intermediate compound loss of -C$_3$O$_2$NH$_4$ and form L6, $m/z = 181.09$. Meanwhile in, compound L5 undergoes degradation to form L7, $m/z = 165.06$, furthermore L6 and L7 compounds can be further defluorination and hydroxylation to form L8, $m/z = 93.06$ [49]. Subsequently, intermediate L8 product might be continues to be broken into small molecule organic acids as well as mineralization product.

4. Conclusion

In conclusion, we have fruitfully fabricate a Sm$_6$WO$_{12}$/g-C$_3$N$_4$ heterojunction photocatalyst by simple and facile strategy. The photocatalytic degradation efficiency of the Sm$_6$WO$_{12}$/g-C$_3$N$_4$ heterojunction
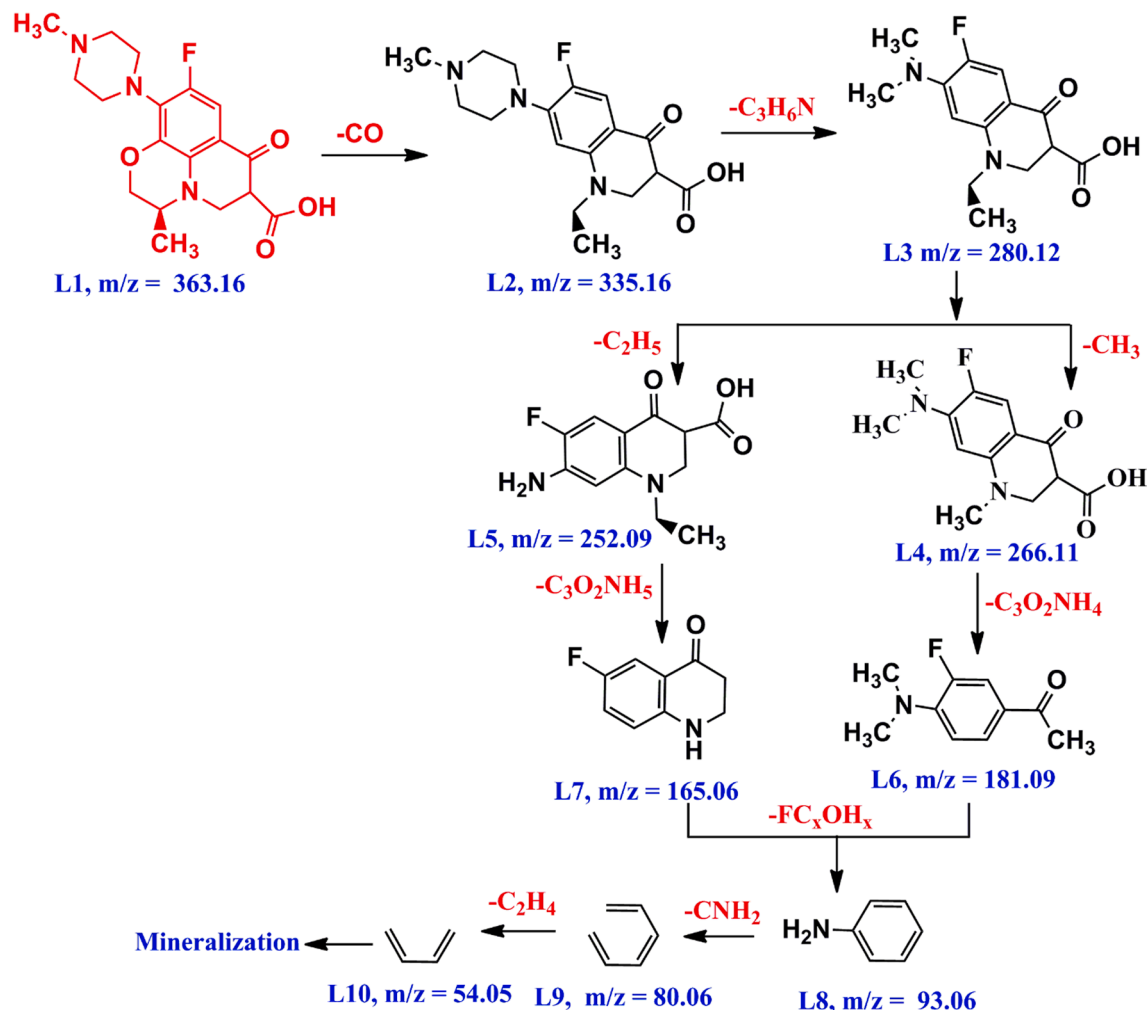

Fig. 10. Proposed degradation pathways of levofloxacin during the photocatalytic reaction.

was greatly boosted, which is about 20.52 and 2.93 times greater than that of single Sm_6WO_{12} and $g-C_3N_4$, respectively. Based on the radical trapping experiments analysis, $O_2^{\bullet-}$ and $^{\bullet}OH$ were proven to be the main reactive species for the degradation of levofloxacin over $Sm_6WO_{12}/g-C_3N_4$ heterojunction. The main intermediates and possible levofloxacin degradation pathways were proposed based on GC–MS results. The admirable photocatalytic efficiency might have been ascribed to the quenched the fast recombination, narrowing bandgap and the massive catalyst active sites. Therefore, this study provides an inspiration for the design of high stability and excellent photocatalyst in the future.

CRediT authorship contribution statement

Seenivasan Laskhmi Prabavathi: Writing - original draft, Conceptualization, Methodology. **Karunamoorthy Saravanakumar:** Methodology, Formal analysis, Investigation. **Chang Min Park:** Investigation, Validation, Writing - review & editing. **Velluchamy Muthuraj:** Conceptualization, Supervision, Writing - review & editing.

Declaration of Competing Interest

The authors declare that they have no known competing financial interests or personal relationships that could have appeared to influence the work reported in this paper.

Acknowledgements

Appendix A. Supplementary material

Supplementary data to this article can be found online at https://doi.org/10.1016/j.seppur.2020.117985.

References

[1] X.J. Wen, C.G. Niu, H. Guo, L. Zhang, C. Liang, G.M. Zeng, Photocatalytic degradation of levofloxacin by ternary $Ag_2CO_3/CeO_2/AgBr$ photocatalyst under visible-light irradiation: degradation pathways, mineralization ability, and an accelerated interfacial charge transfer process study, J. Catal. 358 (2018) 211–223.

[2] Q. Chen, Y. Xin, X. Zhu, Au-Pd nanoparticles-decorated TiO_2 nanobelts for photocatalytic degradation of antibiotic levofloxacin in aqueous solution, Electrochim. Acta 186 (2015) 34–42.

[3] X.C. Liu, D.X. Yang, Y.Y. Zhou, J.C. Zhang, L. Luo, S.J. Meng, S. Chen, M.J. Tan, Z.C. Li, L. Tang, Electrocatalytic properties of N-doped graphite felt in electro Fenton process and degradation mechanism of levofloxacin, Chemosphere 182 (2017) 306–315.

[4] S.L. Prabavathi, K. Govindan, K. Saravanakumar, A. Jang, V. Muthuraj, Construction of heterostructure $CoWO_4/g-C_3N_4$ nanocomposite as an efficient visible-light photocatalyst for norfloxacin degradation, J. Ind. Eng. Chem. 80 (2019) 558–567.

[5] S.M. Derazkola, M.S. Niasari, O. Amiri, A. Abbasi, Fabrication and characterization of $Fe_3O_4@SiO_2@TiO_2@Ho$ nanostructures as a novel and highly efficient photocatalyst for degradation of organic pollution, J. Energy Chem. 26 (2017) 17–23.

[6] F. Motahari, M.R. Mozdianfard, F. Soofivand, M.S. Niasari, NiO nanostructures: synthesis, characterization and photocatalyst application in dye pollution wastewater treatment, RSC Adv. 4 (2014) 27654–27660.

[7] A.R. Vartooni, M. Nasrollahzadeh, M.S. Niasari, M. Atarod, Photocatalytic degradation of azo dyes by titanium dioxide supported silver nanoparticles prepared by a green method using Carpobrotus acinaciformis extract, J. Alloys Compd. 689 (2016) 15–20.

[8] K. Saravanakumar, R. Karthik, S.M. Chen, J. Vinoth Kumar, K. Prakash, V. Muthuraj, Construction of novel $Pd/CeO_2/g-C_3N_4$ nanocomposites as efficient visible-light photocatalysts for hexavalent chromium detoxifcation, J. Colloid Interface Sci. 504 (2017) 514–526.

[9] M. Ghanbari, M.S. Niasari, Tl_4CdI_6 nanostructures: facile sonochemical synthesis and photocatalytic activity for removal of organic dyes, Inorg. Chem. 57 (2018) 11443–11455.

[10] K. Govindan, H.T. Chandran, M. Raja, S.U. Maheswari, M. Rangarajan, Electron scavenger-assisted photocatalytic degradation of amido black 10B dye with Mn_3O_4

nanotubes: a response surface methodology study with central composite design, J. Photochem. Photobiol. A 341 (2017) 146–156.

[11] Y. Song, J. Gu, K. Xia, J. Yi, H. Chen, X. She, Z. Chen, C. Ding, H. Li, H. Xu, Construction of 2D $SnS_2/g-C_3N_4$ Z-scheme composite with superior visible-light photocatalytic performance, Appl. Surf. Sci. 467–468 (2019) 56–64.

[12] Y. Orooji, M. Ghanbari, O. Amiri, M.S. Niasari, Facile fabrication of silver iodide/ graphitic carbon nitride nanocomposites by notable photo-catalytic performance through sunlight and antimicrobial activity, J. Hazard. Mater. 389 (2020), 122079.

[13] S. Lakshmi Prabavathi, K. Saravanakumar, G. Mamba, V. Muthuraj, $1D/2D$ $MnWO_4$ nanorods anchored on $g-C_3N_4$ nanosheets for enhanced photocatalytic degradation ofloxacin under visible light irradiation, Colloids Surf A. 581 (2019), 123845.

[14] Y. Fu, T. Huang, B. Jia, J. Zhu, X. Wang, Reduction of nitrophenols to aminophenols under concerted catalysis by $Au/g-C_3N_4$ contact system, Appl. Catal. B 202 (2017) 430–437.

[15] Y. Li, Z. Ruan, Y. He, J. Li, K. Li, Y. Jiang, X. Xu, Y. Yuan, K. Lin, In-situ fabrication of hierarchically porous $g-C_3N_4$ and understanding on its enhanced photocatalytic activity based on energy absorption, Appl. Catal. B 236 (2018) 64–75.

[16] J.C. Wang, C.X. Cui, Y. Li, L. Liu, Y.P. Zhang, W. Shi, Porous Mn doped $g-C_3N_4$ photocatalysts for enhanced synergetic degradation under visible-light illumination, J. Hazard. Mater. 339 (2017) 43–53.

[17] Q. Han, B. Wang, J. Gao, Z. Cheng, Y. Zhao, Z. Zhang, L. Qu, Atomically thin mesoporous nanomesh of graphitic C_3N_4 for high-efficiency photocatalytic hydrogen evolution, ACS Nano 10 (2016) 2745–2751.

[18] T. Giannakopoulou, I. Papailias, N. Todorova, N. Boukos, Y. Liu, J. Yu, C. Trapalis, Tailoring the energy band gap and edges' potentials of $g-C_3N_4/TiO_2$ composite photocatalysts for NO_x removal, Chem. Eng. J. 310 (2) (2017) 571–580.

[19] V. Jayaraman, A. Mani, Interfacial coupling effect of high surface area Pyrochlore like $Ce_2Zr_2O_7$ over 2D $g-C_3N_4$ sheet photoactive material for efficient removal of organic pollutants, Sep. Purif. Technol. 235 (2020), 116242.

[20] K. Huang, Y. Hong, X. Yan, C. Huang, J. Chen, M. Chen, W. Shi, C. Liu, Hydrothermal synthesis of $g-C_3N_4/CdWO_4$ nanocomposite and enhanced photocatalytic activity for tetracycline degradation under visible light, Cryst. Eng. Comm. 18 (34) (2016) 6453–6463.

[21] C. Li, S. Yu, H. Dong, C. Liu, H. Wu, H. Che, G. Chen, Z-scheme mesoporous photocatalyst constructed by modification of Sn_3O_4 nanoclusters on $g-C_3N_4$ nanosheets with improved photocatalytic performance and mechanism insight, Appl. Catal. B 238 (2018) 284–293.

[22] G. Li, B. Wang, J. Zhang, R. Wang, H. Liu, Rational construction of a direct Z-scheme $g-C_3N_4/CdS$ photocatalyst with enhanced visible light photocatalytic activity and degradation of erythromycin and tetracycline, Appl. Surf. Sci. 478 (2019) 1056–1064.

[23] F. Guo, W. Shi, M. Li, Y. Shi, H. Wen, $2D/2D$ Z-scheme heterojunction of $CuInS_2/g-C_3N_4$ for enhanced visible-light-driven photocatalytic activity towards the degradation of tetracycline, Sep. Purif. Technol. 210 (2019) 608–615.

[24] S. Khademolhoseini, M. Goudarzi, Nanocrystalline samarium tungstate: facile morphology-controlled preparation, characterization and investigation of optical and photocatalytic properties, J. Mater. Sci: Mater. Electron. 28 (2) (2016) 1253–1258.

[25] A.S. Nasab, H. Naderi, M.R. Nasrabadi, M.R. Ganjali, Evaluation of supercapacitive behavior of samarium tungstate nanoparticles synthesized via sonochemical method, J. Mater. Sci.: Mater. Electron. 28 (12) (2017) 8588–8595.

[26] J. Wang, Z.J. Zhang, J.T. Zhao, H.H. Chen, X.X. Yang, Y. Tao, Luminescent metastable $Y_2WO_6:Ln^{3+}$ (Ln = Eu, Er, Sm, and Dy) microspheres with controllable morphology via self-assembly, J. Mater. Chem. 20 (2010) 10894–10900.

[27] Y.H. Li, J.F. Huang, J.Y. Li, L.Y. Cao, J. Lu, J.P. Wu, A hydrothermal assisted method to prepare Samarium Tungstate sheets at lowered reaction temperature, Mater. Lett. 135 (2014) 168–171.

[28] N. Tian, H. Huang, Y. Zhang, Mixed calcination synthesis of $CdWO_4/g-C_3N_4$ heterojunction with enhanced visible-light-driven photocatalytic activity, Appl. Surf. Sci. 343–349 (2015).

[29] L. Ge, C. Han, J. Liu, Novel visible light-induced $g-C_3N_4/Bi_2WO_6$ composite photocatalysts for efficient degradation of methyl orange, Appl. Catal. B Environ. 108–109 (2011) 100–107.

[30] M.S. Seyed Dorraji, A.R. Amani-Ghadim, M.H. Rasoulifard, H. Daneshvar, B. Sistani, Z. Aghdam, A.R. Tarighati, S.F. Hosseini, Photocatalytic activity of $g-C_3N_4$: An empirical kinetic model, optimization by neuro-genetic approach and identification of intermediates, Chem. Eng. Res. Des. 127 (2017) 113–125.

[31] M.G. Arani, M.M. Arani, M.S. Niasari, Facile synthesis, characterization and optical properties of copper vanadate nanostructures for enhanced photocatalytic activity, J. Mater. Sci: Mater. Electron. 27 (2016) 4871–4878.

[32] S.Z. Ajabshir, M.S. Niasari, Z.Z. Ajabshir, $Nd_2Zr_2O_7-Nd_2O_3$ nanocomposites: New facile synthesis, characterization and investigation of photocatalytic behaviour, Mater. Lett. 180 (2016) 27–30.

[33] I.A. Abdelhafeez, J. Chen, X. Zhou, Scalable one-step template-free synthesis of ultralight edge-functionalized $g-C_3N_4$ nanosheets with enhanced visible light photocatalytic performance, Sep. Purif. Technol. 250 (2020), 117085.

[34] J. Li, E.Z. Liu, Y.N. Ma, X.Y. Hu, J. Wan, L. Sun, J. Fan, Synthesis of $MoS_2/g-C_3N_4$ nanosheets as 2D heterojunction photocatalysts with enhanced visible light activity, Appl. Surf. Sci. 364 (2016) 694–702.

[35] P. Xia, B. Zhu, B. Cheng, J. Yu, J. Xu, $2D/2D$ $g-C_3N_4/MnO_2$ nanocomposite as a direct Z-scheme photocatalyst for enhanced photocatalytic activity, ACS Sustain. Chem. Eng. 6 (1) (2017) 965–973.

[36] Z. Liu, J. Tian, D. Zeng, C. Yu, L. Zhu, W. Huang, K. Yang, D. Li, A facile microwave-hydrothermal method to fabricate B doped $ZnWO_4$ nanorods with high crystalline and highly efficient photocatalytic activity, Mater. Res. Bull. 94 (2017) 298–306.

[37] T. Xiao, Z. Tang, Y. Yang, L. Tang, Y. Zhou, Z. Zou, In situ construction of hierarchical WO_3/g-C_3N_4 composite hollow microspheres as a Z-scheme photocatalyst for the degradation of antibiotics, Appl. Catal. B 220 (2018) 417–428.

[38] K. Saravanakumar, M.M. Ramjan, P. Suresh, V. Muthuraj, Fabrication of highly efficient visible light driven Ag/CeO_2 photocatalyst for degradation of organic pollutants, J. Alloy. Compds 664 (2016) 149–160.

[39] M. Humayun, Z. Hu, A. Khan, W. Cheng, Y. Yuana, Z. Zheng, Q. Fu, W. Luo, Highly efficient degradation of 2, 4-dichlorophenol over CeO_2/g-C_3N_4 composites under visible-light irradiation: Detailed reaction pathway and mechanism, J. Hazard. Mater 364 (2019) 635–644.

[40] Y. Guo, J. Li, Z. Gao, X. Zhu, Y. Liu, Z. Wei, W. Zhao, C. Sun, A simple and effective method for fabricating novel p–n heterojunction photocatalyst g-C_3N_4/$Bi_4Ti_3O_{12}$ and its photocatalytic performances, Appl. Catal. B 192 (2016) 57–71.

[41] K. Saravanakumar, V. Muthuraj, S. Vadivel, Constructing novel Ag nanoparticles anchored on MnO_2 nanowires as an efficient visible light driven photocatalyst, RSC Adv. 6 (2016) 61357–61366.

[42] K. Govindan, A.K. Suresh, T. Sakthivel, M. Kalpana, M. Raja, V. Gunasekaran, A. Jang, Effect of peroxomonosulfate, peroxodisulfate and hydrogen peroxide on graphene oxide photocatalytic performances in methyl orange dye degradation, Chemosphere 237 (2019), 124479.

[43] S. Sharma, A. Umar, S.K. Mehta, A.O. Ibhadon, S.K. Kansal, Solar light driven photocatalytic degradation of levofloxacin using TiO_2/carbon-dot nanocomposites, New J. Chem. 42 (9) (2018) 7445–7456.

[44] G. Gupta, A. Kaur, A.S.K. Sinha, S.K. Kansal, Photocatalytic degradation of levofloxacin in aqueous phase using Ag/AgBr/BiOBr microplates under visible light, Mater. Res. Bull. 88 (2017) 148–155.

[45] A. Kaur, S.K. Kansal, Bi_2WO_6 nanocuboids: An efficient visible light active photocatalyst for the degradation of levofloxacin drug in aqueous phase, Chem. Eng. J. 302 (2016) 194–203.

[46] M. Jourshabani, Z. Shariatinia, A. Badiei, Synthesis and characterization of novel Sm_2O_3/S-doped g-C_3N_4 nanocomposites with enhanced photocatalytic activities under visible light irradiation, Appl. Surf. Sci. 427 (2018) 375–387.

[47] S.L. Prabavathi, K. Saravanakumar, T.T.I. Nkambule, V. Muthuraj, G. Mamba, Enhanced photoactivity of cerium tungstate modified graphitic carbon nitride heterojunction photocatalyst for the photodegradation of moxifloxacin, J. Mater. Sci: Mater. Electron. 31 (2020) 11434–11447.

[48] Y. Gong, J. Li, Y. Zhang, M. Zhang, X. Tian, A. Wang, Partial degradation of levofloxacin for biodegradability improvement by electro-Fenton process using an activated carbon fiber felt cathode, J. Hazard. Mater. 304 (2016) 320–328.

[49] A. Dwivedi, S.F. Mujtaba, H.N. Kushwaha, D. Ali, N. Yadav, S. Singh, R.S. Ray, Photosensitizing mechanism and identification of levofloxacin photoproducts at ambient UV radiation, Photochem. Photobiol. 88 (2012) 344–355.

[50] B.S.M. Al Balushi, F. Al Marzouqi, B. Al Wahaibi, A.T. Kuvarega, S.M.Z. Al Kindy, Y. Kim, R. Selvaraj, Hydrothermal synthesis of CdS sub-microspheres for photocatalytic degradation of pharmaceuticals, Appl. Surf. Sci. 457 (2018) 559–565.

[51] S.K. Kansal, P. Kundu, S. Sood, R. Lamba, A. Umar, S.K. Mehta, Photocatalytic degradation of antibiotic levofloxacin using well-crystalline TiO_2 nanoparticles, New J. Chem. 38 (2014) 3220–3226.

[52] A. Kaur, D. Salunke, A. Umar, S.K. Mehta, A.S.K. Sinha, S. Kansal, Visible light driven photocatalytic degradation of fluoroquinolone levofloxacin drug using Ag_2O/TiO_2 quantum dots: A mechanistic study and degradation pathway New, J. Chem. 41 (2017) 12079–12090.

[53] G. Lu, Z. Lun, H. Liang, H. Wang, Z. Li, W. Ma, In situ fabrication of $BiVO_4$-$CeWO_4$ heterojunction for excellent visible light photocatalytic degradation of levofloxacin, J. Alloys compd. 772 (2019) 122–131.